

780 nm Compact Optical Clock Down-Conversion for Microwave Frequencies with 10^{-14} instability

Zhendong Chen^a, Tianyu Liu^a, Qiaohui Yang^a, Ya Wang^a, Jie Miao^a, Jingming Chen^a, Duo Pan^{a*}, Ruao Yang^{a*}, Jianjun Wu^a, Zhigang Zhang^a, and Jingbiao Chen^{a,b}

^a State Key Laboratory of Advanced Optical Communication Systems and Networks, School of Electronics, Peking University, Beijing 100871, China

^b Hefei National Laboratory, Hefei 230088, China

* Corresponding author: panduo@pku.edu.cn ruao.yang@pku.edu.cn

ABSTRACT

We demonstrated a compact rubidium optical clock, which includes an optical frequency standard and an optical frequency comb, with an optical path volume of merely 11.6 liters. The laser frequency is stabilized to the hyperfine transitions of the rubidium D2 line using modulation transfer spectroscopy (MTS), which eliminates Doppler background and provides a high signal to noise ratio and high sensitivity. A 300 MHz microwave signal, whose phase exactly tracks that of the optical frequency standard (OFC), is generated via the optical frequency comb, yielding a frequency instability of $1.89 \text{ E-}13 @ 1 \text{ s}$ and $5.27 \text{ E-}14 @ 1000 \text{ s}$ in the electronic domain. To the best of our knowledge, this is the first optical clock at Rb D2 line. These results offer a promising approach for the development of portable optical clock.

1. Introduction

Optical clocks, with optical frequency standards and optical frequency combs (OFC) as fundamental components, find wide-ranging applications in transportation, telecommunications, and cloud computing.¹⁻⁶ In 2011, The National Institute of Standards and Technology (NIST) realized an optical clock based on Yb atoms, achieving frequency instability in microwave range of better than 10^{-18} , which represents an improvement by two orders of magnitude over the best microwave clocks.⁷ Optical clocks can be classified into two primary categories based on their application scope: high-precision transportable optical clocks, which offer extremely accurate measurements, and portable optical clocks, which prioritize mobility and convenience.⁸⁻¹⁰

To conduct cutting-edge physical research and measurements, such as gravitational redshift, gravitational wave detection, and dark matter exploration, it is necessary to integrate and protect complex, high-precision atomic clocks and transport them to the application site.^{11,14} It has been reported that there is much research on high-precision portable optical clocks, utilizing atomic systems that include neutral atom optical lattices and single ion systems in recent years. In 2017, the German Federal Institute of Physics and Technology (PTB) achieved the first portable strontium optical lattice clock for long-distance vehicle transportation and measurement applications, the overall dimensions of the system are $2.2 \text{ m} \times 3 \text{ m} \times 2.2 \text{ m}$, the stability is $1.3 \text{ E-}15 / \sqrt{\tau}$, and the uncertainty is $7.41 \text{ E-}17$.¹¹ In 2020, the RIKEN successfully developed a high-precision transportable optical lattice clock, which was then placed at the top of the 450-meter Tokyo Skytree to compare with a ground-based optical clock. This work also demonstrated that optical clocks can be technically used for field applications such as crustal deformation and geoid testing, achieving a resolution at the centimeter level.¹²

Portable optical clocks, while maintaining a compact size, have performance that can now rival that of commercial atomic clocks.¹⁵⁻²⁰ The current research is mainly focused on the development of thermal atomic/molecular gas cell optical clocks, which primarily include small optical clocks based on frequency stabilization using iodine molecules and alkali metal atomic gas cells. In 2020, the NIST reported a compact, portable optical clock based on rubidium atoms at 778 nm, this miniature device, leveraging two-photon transition technology, boasts a volume of approximately 35 cm^3 , and an impressive stability of $2.9 \text{ E-}12 @ 1 \text{ s}$.¹⁹ In 2024, the iodine optical clocks developed by NIST operated continuously aboard a naval ship in the Pacific Ocean for 20 days, with timing errors accumulating to less than 300 picoseconds per day.²⁰

Currently, portable optical clocks are predominant based on Rb two-photon transition optical standards, with no realization yet of a Rb/Cs first excited state transition clock, despite its potential advantages in terms of easier implementation and integration. In this work, we present the first 780 nm optical clock based on the Rb D2 transition. The optical frequency standard is locked to the 780 nm $5S_{1/2} F=2 \rightarrow 5P_{3/2} F'=3$ transition of 87Rb using MTS. To achieve miniaturization of the optical clock, a tailored OFC based on fiber lasers has also been specifically designed, and the tracking frequency stability is better than $\text{E-}17$, with an carrier-envelope offset frequency (f_{ceo}) stability of $7.86 \text{ E-}18 @ 1 \text{ s}$ and a beat frequency stability (f_{beat}) of $1.01 \text{ E-}17 @ 1 \text{ s}$. The integrated OFC faithfully transfers the clocks' optical frequency stability into its RF outputs, with short-term stability reaching $1.89 \text{ E-}13 @ 1 \text{ s}$, the long-term stability reaching $5.27 \text{ E-}14 @ 1000 \text{ s}$.

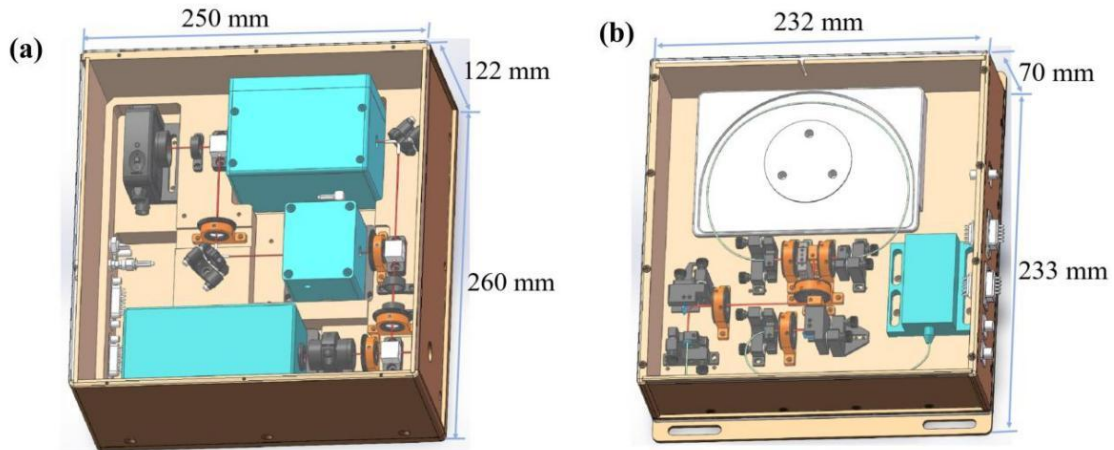


Fig. 1. (a) Experimental setup of optical frequency standard based MTS system. (b) Experimental setup of optical frequency comb based Erbium-doped fiber laser

2. Experimental methods

Fig. 1 shows the experimental setup images for both the optical frequency standard and the OFC. To enhance mechanical stability, all components are firmly attached to an aluminum baseboard, and the entire setup is enclosed during operation to minimize the impact of external disturbances.

The schematic of the 780-nm laser system frequency stabilized by MTS is shown in Fig. 2(a). A 780-nm interference filter configuration external cavity diode laser is used as the local oscillator for optical frequency standard, its frequency is controlled by adjusting the injection current and the piezoelectric transducer (PZT). The laser, after traversing an isolator and a beam expander, emits a beam at 780.246 nm, which is split by two PBS into two beams: one for the pump and the other for the probe. The power ratio between the pump light and the probe light can be adjusted by rotating the two wave plates in the optical path. By rotating the wave plate, the polarization direction of the pump beam is aligned with the axis of the electro-optic crystal. To reduce the residual amplitude modulation of the EOM, an EOM with beveled edges is used, and the temperature of the EOM is controlled by a stabilization controller (Thorlabs TC200C). The pump light is phase-modulated by an EOM, then enters a $\phi 10 \text{ mm} \times 50 \text{ mm}$ cylindrical glass cell filled with 87Rb atoms through reflection. The probe light directly enters the gas cell and overlaps with the pump light in the opposite direction. The gas cell is wrapped with multiple layers of teflon for heat insulation and enclosed in a double-layer cylindrical permalloy for magnetic shielding. Simultaneously, the temperature of the rubidium atomic vapor cell is

monitored by a thermistor, and then regulated by a temperature controller (Thorlabs TC300), which in turn adjusts the current sent to the heater accordingly. The MTS optical system is enclosed in a metal box, which is wrapped in teflon, with a total volume of 7.8 L.

The modulation transfer process takes place within the rubidium atomic vapor cell. The probe light is detected by the photodetector, and the resulting signal is the saturated absorption spectrum (SAS) signal. The mixer demodulates the signal to obtain the MTS signal. This signal is used as the error signal for the PID locking system to lock the laser frequency onto the atomic transition. The rubidium atom is selected as a quantum reference as shown in Fig. 2(b), and the 780 nm laser is locked to the 87Rb fine level $5S_{1/2} F=2 \rightarrow 5P_{3/2} F'=3$ clock transition by the driving current and the PZT.

The experimental setup of the entire optical clock system is shown in Fig. 3, the optical path is represented by red lines, and the electrical circuit is represented by gray lines. The femtosecond laser source is a home-made Er: fiber laser based on nonlinear polarization evolution (NPE) mode-locking mechanisms. The output power of the laser is 280 mW and the fundamental repetition rate is up to 282 MHz. The net dispersion of the laser cavity is designed to be close to zero to achieve stretched-pulse operation, thereby achieving lower noise levels. An EOM and a PZT attached to the fiber, serving as feedback devices, are installed in the laser. The oscillator is placed in an aluminum box wrapped in thermal insulation, with thermoelectric coolers (TECs) located underneath the inner aluminum box.

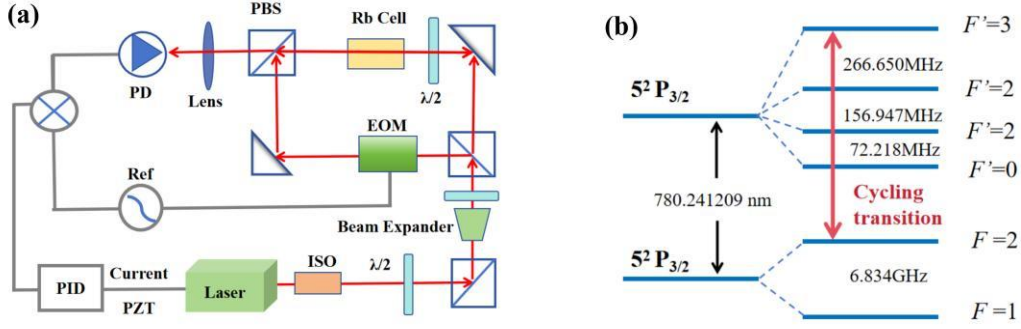


Fig. 2. (a) Experimental setup of the MTS system: ISO is a space isolator, $\lambda/2$ is a half-wave plate, PZT is a piezoelectric transducer, PBS is a polarizing beam splitter, EOM is an electro-optic modulator, PD is a photodetector. (b) The hyperfine levels of the ^{87}Rb D2 transition.

The laser output from the laser source is bifurcated into two branches by the PBS. One beam is used to obtain the f_{ceo} , and another beam is used to beat with the optical frequency standard. To meet the requirements for spectral broadening, we designed and constructed an erbium-doped fiber amplifier (EDFA). By optimizing the amplifier, the output power is achieved at 120 mW, and the pulse width is 69 fs, which results in the best spectral broadening effect. Then, the amplified pulses are coupled to a f-to-2f waveguide module based on a tantalum pentoxide (Octave Photonics, COSMO). The pulses are spread to the octave range in the waveguide module, and the f_{ceo} is obtained by doubling the frequency. The f_{ceo} signal is first filtered through a band-pass filter (BPF) to reduce background noise, then amplified by an amplifier before entering the phase-locking circuit. The pump current of the oscillator is controlled by the locking circuit to stabilize the f_{ceo} signal. The second beam of femtosecond laser source is amplified to 150 mW by another EDFA. Then,

the laser at 1560 nm undergoes frequency doubling through a periodically-poled lithium niobate crystal doped with magnesium oxide (MgO: PPLN), the period of the PPLN crystal is 19.60 μm . To achieve higher frequency doubling efficiency, a focusing lens and a collimating lens are placed at the front and back of the crystal, respectively. An output of 8 mW at a wavelength of 780 nm can be achieved using the PPLN crystal. The optical frequency standard outputs a 780 nm laser, which is collimated and adjusted with a lens to match the spot size of the OFC's light. Two light beams are combined using a polarizing beam splitter (PBS), while wave plates are fine-tuned to generate a beat frequency signal. The beat frequency signal is locked to the optical frequency standard using a phase-locked loop circuit. A PZT functions as the slow loop, while an EOM acts as the fast loop for fine-tuning the OFC. As a result, the OFC is stabilized to the optical frequency standard, forming an integrated optical clock system.

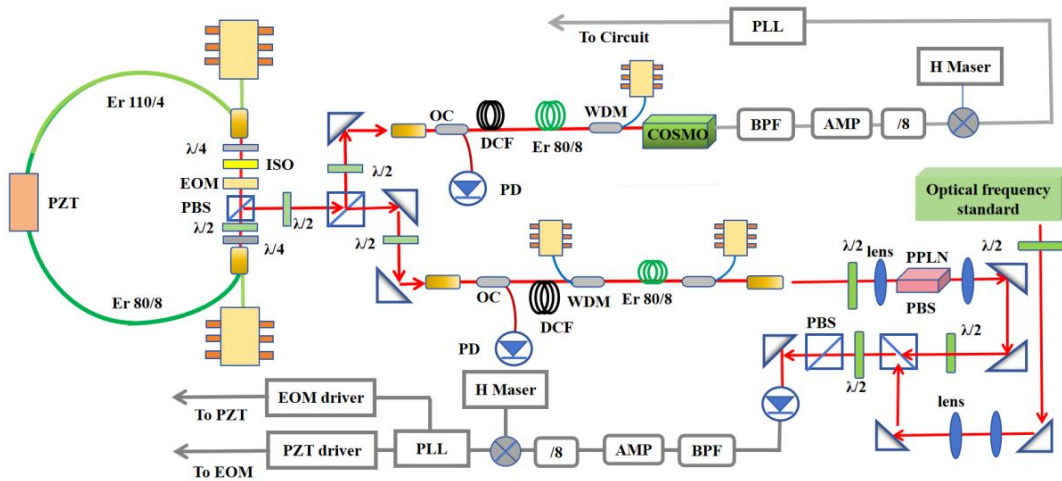


Fig. 3. The structure of the Rubidium Optical Clock. ISO is a space isolator, $\lambda/4$ is a quarter-wave plate, $\lambda/2$ is a half-wave plate, PZT is a piezoelectric transducer, WDM is wavelength division multiplexing component, PBS is a polarizing beam splitter, PC is a polarization controller, EOM is an electro-optic modulator, PD is a photodetector, PPLN is a frequency conversion crystal, H-maser is a microwave reference, AMP is a microwave amplifier, BPF is a band-pass filter, and PLL is a phase lock loop.

3. Results and discussion

The shape of the MTS line varies with different gas cell temperatures and modulation frequencies. The slope at the center point of the demodulation signal reflects the demodulation sensitivity of the spectral line. At a modulation frequency of 9.62 MHz and a gas cell temperature of 37.08 °C, the modulation transfer spectrum achieves its maximum slope of 542 mV/MHz. The quantum reference spectrum is depicted in Fig. 4(a), where the blue curve

represents the SAS signal directly detected by the PD, and the red curve represents the MTS signal. Based on the frequency discrimination signal obtained from the MTS, we lock the laser frequency to the D2 line of ^{87}Rb through optimizing PID circuit parameters. Fig. 4. (b) shows the data of the beat frequency between the commercial OFC and optical frequency standard. The true value of the optical frequency standard, determined based on the OFC's repetition frequency and f_{ceo} , is 384,228,115,588.473 KHz.

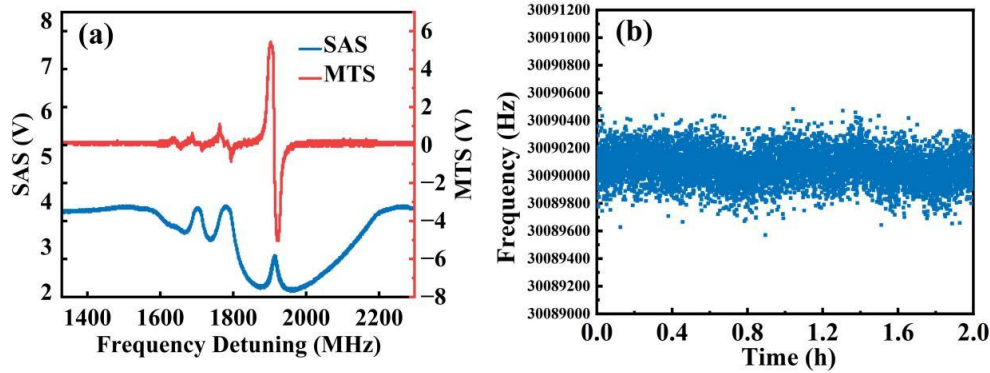


Fig. 4. (a) Spectra signals of modulation transfer spectrum (red line) and saturated absorption spectroscopy (blue line). (b) the fluctuations of the f_{beat} signal between the commercial OFC and optical frequency standard.

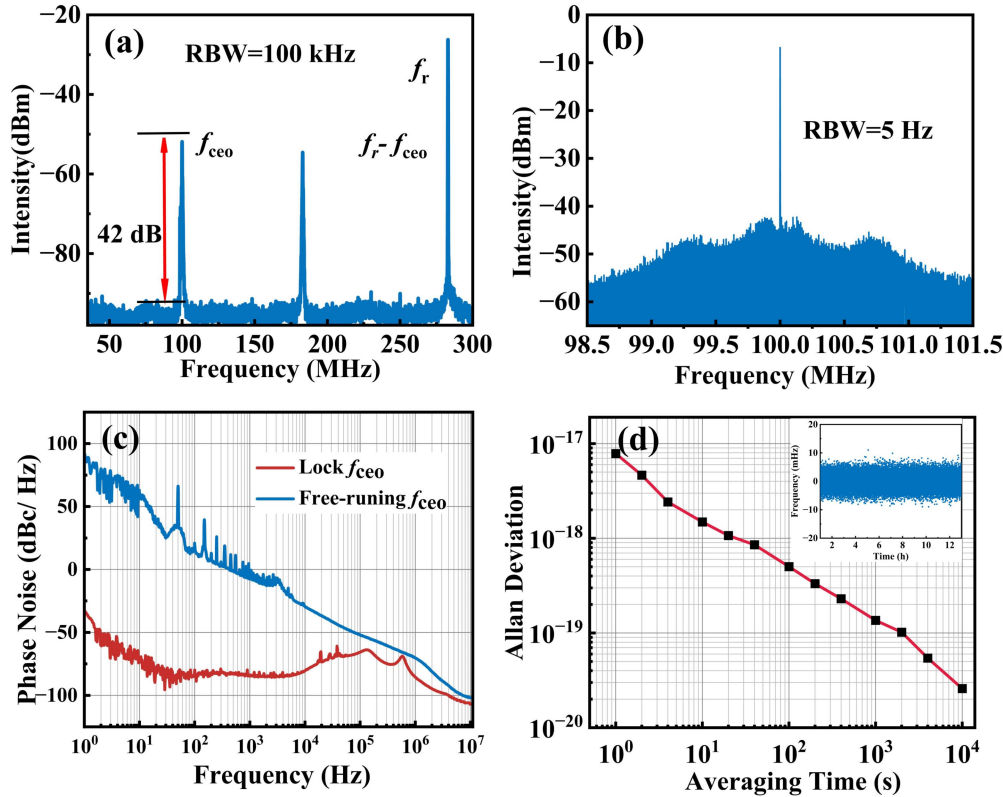


Fig. 5. (a) Radio frequency of free-running f_{ceo} . (b) Radio frequency of phase-locked f_{ceo} . (c) Power spectral density of free-running f_{ceo} (blue) and phase-locked f_{ceo} (red). (d) Frequency stability of phase-locked f_{ceo} . Inset: the fluctuations of the phase-locked f_{ceo} signal for about 12 hours.

To convert the optical frequency of the rubidium atomic frequency standard into microwaves, the home-made OFC must first be locked. The hydrogen clock signal serves as the microwave reference signal for the OFC. As shown in Fig. 5 (a), the signal-to-noise ratio of the free running f_{ceo} is estimated to be 41 dB at a resolution bandwidth of 100 kHz. The f_{ceo} signal is locked to 100 MHz by reasonably optimizing the parameters of the locking circuit. Based on the servo peak, the servo bandwidth is estimated to be 710 kHz, and signal-to-noise ratio is 37 dB - see Fig. 5 (b). Fig. 5 (c) shows the phase noise of the f_{ceo} under the free running and

the locked conditions. The phase noise is effectively reduced through phase-locking, with a substantial decrease from 92 dBc/Hz to -33 dBc/Hz at a 1 Hz frequency offset. The integrated phase noise of the locked f_{ceo} is 388 mrad, integrated over the range from 10 MHz to 1 Hz. The frequency count of the locked f_{ceo} signal are recorded for 12 hours, with a standard deviation of 2.33 mHz, as depicted in the illustration of Fig. 5 (d). To demonstrate the stability of f_{ceo} , we calculated the Allan deviation based on the data, the frequency stability is $7.86 \text{ E}-18$ at 1s, and drops to $2.59 \text{ E}-20$ at 10000 s.

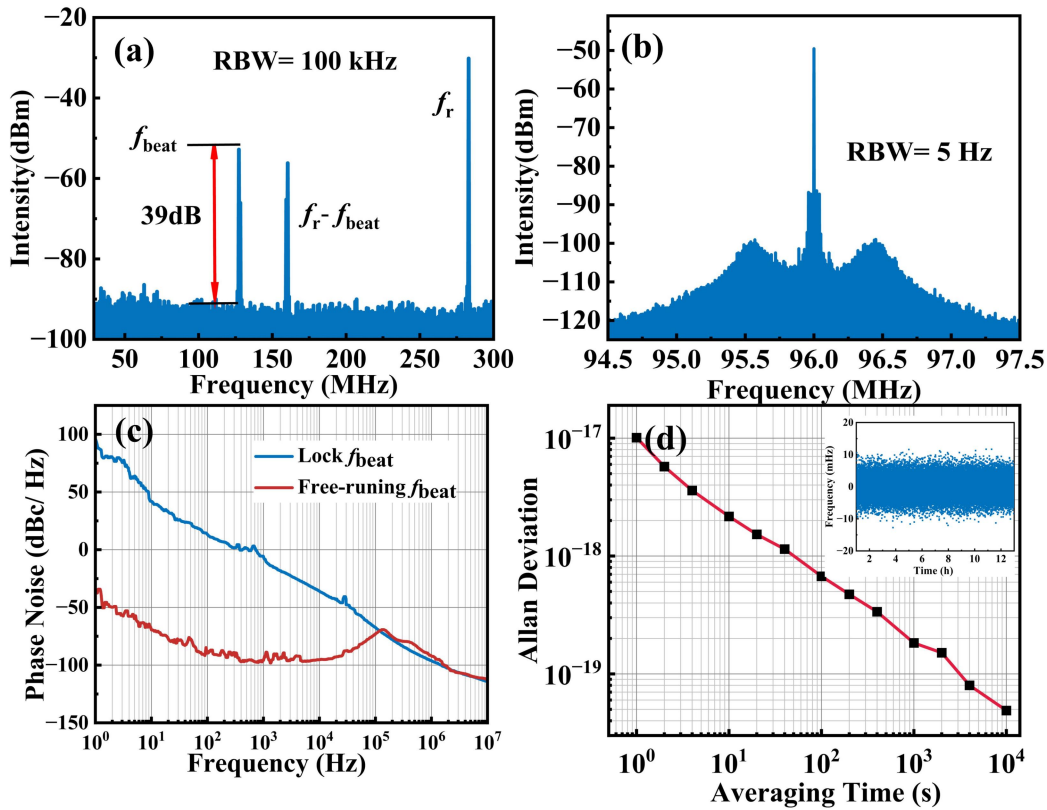


Fig. 6. (a) Radio frequency of free-running f_{beat} . (b) Radio frequency of phase-locked f_{beat} . (c) Power spectral density of free-running f_{beat} (blue) and phase-locked f_{beat} (red). (d) Frequency stability of phase-locked f_{beat} . Inset: the fluctuations of the phase-locked f_{beat} signal for about 12 hours.

It is found that the higher the beat frequency signal-to-noise ratio, the easier the lock can be achieved. By optimally adjusting the spot sizes and the overlap of the two optical beams, the signal-to-noise ratio of the free running f_{beat} can reach up to 39 dB - see Fig. 6(a). An EOM is used for fast loop control, and a PZT is used for slow loop control, after locking, the signal-to-noise ratio f_{beat} is 55 dB, and the servo bandwidth can be increased to 450 kHz by adjusting the PID parameters as shown in Fig. 6(b). Fig. 6(c)

illustrates the phase noise of the f_{beat} , which is well suppressed by phase-locking, the RMS noise of phase-locked f_{beat} is 358 mrad with an integration range from 10 MHz to 1 Hz. The stability of f_{beat} signal is depicted in Fig. 6 (d), the Allan Deviation is $1.01 \text{ E}-17$ at 1 s gate time. The data from the continuous counting of the counter over a 12-hour period is shown in the illustration, and the standard deviation is calculated to be 3.04 mHz. Therefore, the OFC tracking stability is quite high, allowing for transferring the stability of the optical clock into the RF domain.

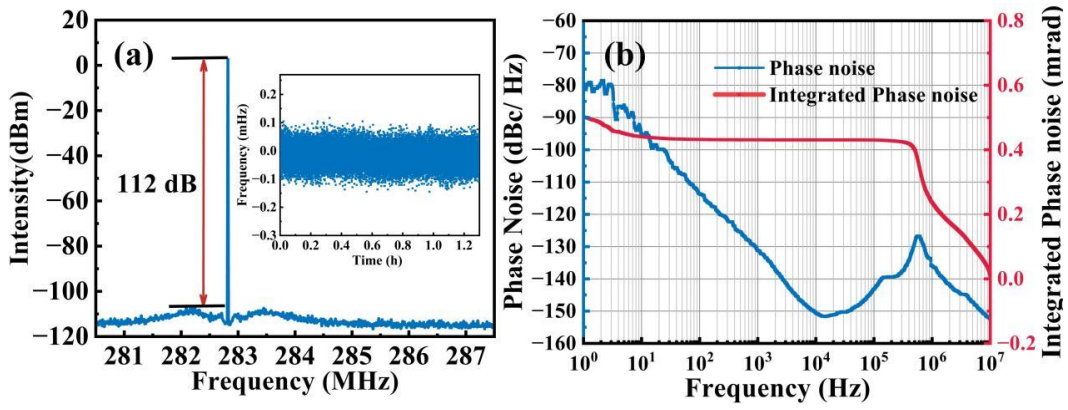


Fig. 7. (a) Radio frequency spectrum of the optical clock signal, inset: the frequency fluctuation of the optical clock signal. (b) Measured phase noise spectrum (blue line) and an integrated (1 Hz-10 MHz) root mean square phase noise (red line).

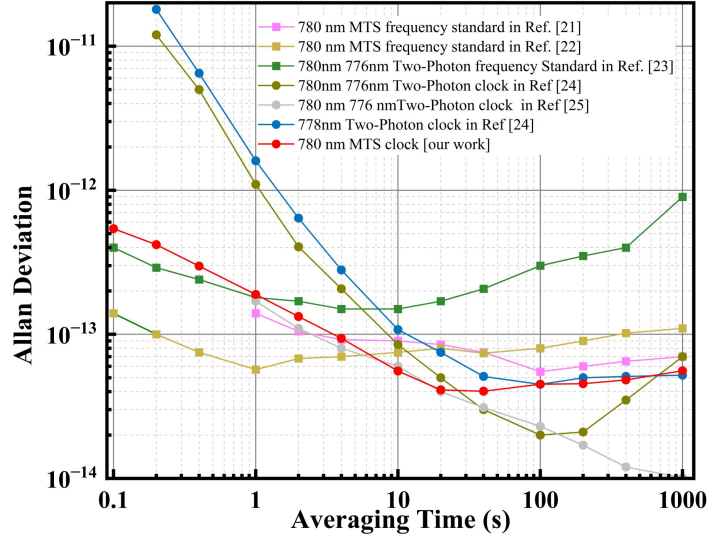


Fig. 8. The frequency stability of the thermal rubidium atomic frequency standards and optical clocks.

Because the OFC is phase locked to the optical frequency standard, the repetition rate of the OFC in the microwave range acquires the stability of the optical frequency standard. The signal-to-noise ratio (SNR) of the microwave signal, as depicted in Fig. 7(a), is 112 dB at a 3 Hz resolution bandwidth (RBW). The illustration in Fig. 7(a) illustrates the microwave frequency data emitted by the optical clock, and the standard deviation is estimated to be 0.033 mHz. The phase noise power spectral density is measured by a phase noise analyzer as shown in Fig. 7(b), the phase-noise spectrum supplements the short-term frequency stability measurements.

As shown in Fig. 8, the short-term stability of this rubidium atomic clock is 1.89×10^{-13} at 1-s gate time, reaching 4.12×10^{-14} at 20-s averaging time, where the Allan deviation then slightly degrades, and does not exceed 5.59×10^{-14} until 1000 s. The stability is highly competitive with previously published thermal rubidium atomic frequency standards and

optical clocks. In addition, unlike the two-photon system that necessitates bulky fluorescence collection equipment, this optical clock utilizing MTS boasts a more compact and portable mechanism.

4. Conclusion

In summary, we report a compact thermal ^{87}Rb optical clock stabilized by MTS for the first time. The volume of the optical clock's light path has been reduced to 11.6 L by optimizing the structure of the optical frequency standard and using a self-made compact OFC. The integrated OFC is phase-locked to the optical frequency standard, thereby faithfully transferring the clocks' optical frequency stability into its RF outputs. The frequency instability reached short-term stability of 1.89×10^{-13} @1s, the long-term stability of 5.59×10^{-14} @1000s. To the best of our knowledge, this is the first optical clock based on the Rb D2 transition. The obtained results provide an alternative method for portable

optical clock and also open the way for extensive applications of optical clock. In future work, we will enhance the long-term stability of the optical clock by employing a superior temperature control system to mitigate temperature fluctuations in the atomic ensemble, as well as by more precisely controlling the temperature of the EOM to reduce residual amplitude modulation.

ACKNOWLEDGMENT

This work is supported by Beijing Nova Program (No. 20240484696); INNOVATION Program for Quantum Science and Technology (2021ZD0303200); Wenzhou Major Science and Technology Innovation Key Project (No. ZG2020046). National Natural Science Foundation of China (U2031208). Boya Postdoctoral Fellowship and Postdoctoral Fellowship Program (GZB20230009).

REFERENCES

- [1] W. F. McGrew, X. Zhang, R. J. Fasano, S. A. Schäffer, K. Beloy, D. Nicolodi, R. C. Brown, N. Hinkley, G. Milani, M. Schioppo, T. H. Yoon, and A. D. Ludlow, Atomic clock performance enabling geodesy below the centimetre level, *Nature* 564, 87 (2018).
- [2] I. Ushijima, M. Takamoto, M. Das, T. Ohkubo, and H. Katori, Cryogenic optical lattice clocks, *Nat. Photonics* 9, 185 (2015).
- [3] S. L. Campbell, R. B. Hutson, G. E. Marti, A. Goban, N. D. Oppong, R. L. McNally, L. Sonderhouse, J. M. Robinson, W. Zhang, B. J. Bloom, and J. Ye, A Fermi-degenerate three-dimensional optical lattice clock, *Science* 358, 90 (2017).
- [4] P. Chang, H. Peng, S. Zhang, Z. Chen, B. Luo, J. Chen, and H. Guo, "A Faraday laser lasing on Rb 1529 nm transition," *Sci. Rep.* 7, 8995 (2017).
- [5] Lemke, N. D., Martin, K. W., Beard, R., Stuhl, B. K., Metcalf, A. J., & Elgin, J. D. (2022). Measurement of optical rubidium clock frequency spanning 65 days. *Sensors*, 22(5), 1982.
- [6] G. Genov, T. E. Lellinger, T. Halfmann, and T. Peters, Laser frequency stabilization by bichromatic saturation absorption spectroscopy, *J. Opt. Soc. Am. B* 34, 2018 (2017).
- [7] J. Bloom, T. L. Nicholson, J. R. Williams, S. L. Campbell, M. Bishof, X. Zhang, W. Zhang, S. L. Bromley, and J. Ye, An optical lattice clock with accuracy and stability at the 10^{-18} level, *Nature* 506, 71 (2014).
- [8] A. D. Ludlow, M. M. Boyd, J. Ye, E. Peik, and P. O. Schmidt, Optical atomic clocks, *Rev. Mod. Phys.* 87, 637 (2015).
- [9] H. Shang, X. Zhang, S. Zhang, D. Pan, H. Chen, and J. Chen, Miniaturized calcium beam optical frequency standard using fully-sealed vacuum tube with 10–15 instability, *Opt. Express* 25, 30459 (2017).
- [10] Z. L. Newman et al., Architecture for the photonic integration of an optical atomic clock, *Optica* 6, 680 (2019).
- [11] Koller, S. B., J. Grotti, St Vogt, A. Al-Masoudi, S. Dörscher, S. Häfner, U. Sterr, and Ch Lisdat. "Transportable optical lattice clock with 7×10^{-17} uncertainty," *Physical review letters* 118, no. 7 (2017): 073601.
- [12] M. Takamoto, I. Ushijima, N. Ohmae, T. Yahagi, K. Kokado, H. Shinkai, H. Katori, "Test of general relativity by a pair of transportable optical lattice clocks," *Nature photonics*, 14(7), 411-415. (2020).
- [13] N. Poli, M. Schioppo, S. Vogt, S. Falke, U. Sterr, C. Lisdat, G. M. Tino. "A transportable strontium optical lattice clock," *Applied Physics B*, 117, 1107-1116(2014).
- [14] S. Origlia, M. S.Pramod, S. Schiller, Y. Singh, K. Bongs, R. Schwarz, C. Lisdat, "Towards an optical clock for space: Compact, high-performance optical lattice clock based on bosonic atoms". *Physical Review A*, 98(5), 053443 (2018).
- [15] K. Döringshoff, T. Schuldt, E. V. Kovalchuk, J. Stühler, C.Braxmaier, A. Peters, "A flight-like absolute optical frequency reference based on iodine for laser systems at 1064 nm," *Applied Physics B*, 123, 1-8. (2017).
- [16] K. Döringshoff, F. B. Gutsch, V. Schkolnik, C. Kürbis, M. Oswald, B. Pröbster, A. Peters, "Iodine frequency reference on a sounding rocket," *Physical Review Applied*, 11(5), 054068.(2019)
- [17] J. X Miao, T. T. Shi , J. B. Chen, "Compact 459-nm Cs Cell Optical Frequency Standard with $2.1 \times 10^{-13} / \sqrt{\tau}$ Short-Term Stability". *Physical Review Applied*, 18, 024034, (2022).
- [18] A. Strangfeld, S. Kanthak, M. Schiemangk, B. Wiegand, A. Wicht, A. Ling, and M. Krutzik, Prototype of a compact rubidium-based optical frequency reference for operation on nanosatellites, *J. Opt. Soc. Am. B* 38, 1885 (2021).
- [19] V. Maurice, Z. L. Newman, S. Dickerson, M. Rivers, J. Hsiao, P. Greene, and C. Johnson, "Miniaturized optical frequency reference for next-generation portable optical clocks," *Optics Express*, 28(17), 24708-24720 (2020).
- [20] J. D. Roslund, A. Cingöz, W. D. Lunden, G. B. Partridge, A. S. Kowligy, F. Roller, and M. M. Boyd, "Optical clocks at sea," *Nature*, 628(8009), 736-740 (2024)
- [21] S. Lee, G. Moon, S. Park, Hong, J. H. Lee, S. Seo, "Laser frequency stabilization in the 10^{-14} range via optimized modulation transfer spectroscopy on the 87Rb D2 line," *Optics letters*, 48 4, 1020-1023 (2023).
- [22] S. Lee, S. B. Lee, S. E. Park, H. G. Hong, G. Moon, "Compact modulation transfer spectroscopy module for highly stable laser frequency," *Optics and Lasers in Engineering*, 146(9), 106698 (2021).
- [23] C. Perrella, P. S. Light, J. D. Anstie, F. N. Baynes, R. T. White, and A. N. Luiten, "Dichroic two-photon rubidium frequency standard," *Physical Review Applied* 12 5, 054063 (2019).
- [24] E. Ahern, J. W. Allison, C. Billington, N. Bourbeau Hébert, A. P. Hilton, E. Klantsataya, C. Locke, "Demonstration of a Mobile Optical Clock Ensemble at Sea," *arXiv preprint arXiv:2406.03716*, (2024).
- [25] E. J. Ahern, S. K. Scholten, C. Locke, N. Bourbeau-Hebert, B. White, A. N. Luiten, "Tailoring the Stability of a Two-Color, Two-Photon Rubidium Frequency Standard," *arXiv preprint arXiv:2410.16654* (2024).